

COMPARISON OF 2- AND 3-PHASE BEARINGLESS SLICE MOTOR CONCEPTS

Franz Zürcher^{*1}, Thomas Nussbaumer^{*2}, Wolfgang Gruber^{*3}, Johann W. Kolar^{*1}
^{*1} ETH Zurich, ^{*2} Levitronix GmbH, ^{*3} ACCM GmbH (J. K. University Linz)

ABSTRACT

Several processes in chemical, pharmaceutical, biotechnology and semiconductor industry require contactless levitation and rotation through a hermetically closed process chamber. A highly interesting topology for these applications is the “bearingless slice motor” concept, where already some research has been done in the past, especially focusing on topology and implementation issues. However, only little work has been done to evaluate the ideal number of motor phases. In this paper, a performance evaluation between 2-phase and 3-phase bearingless slice motor concepts is undertaken. It is shown, that 3-phase systems can supply almost the same power as adequate 2-phase systems and achieve nearly the same acceleration behavior, although they have significantly less complex power electronics.

INTRODUCTION

Bearingless slice motors [1] have gained a lot of attractiveness during the last years for industry branches such as semiconductor, biotechnology and chemical industry, where spinning processes in a high-purity environment have to be performed [2],[3]. A typical configuration of the bearingless motor for these spinning applications is depicted in Figure 1, where the levitating rotor carries a process object and is hermetically sealed in a

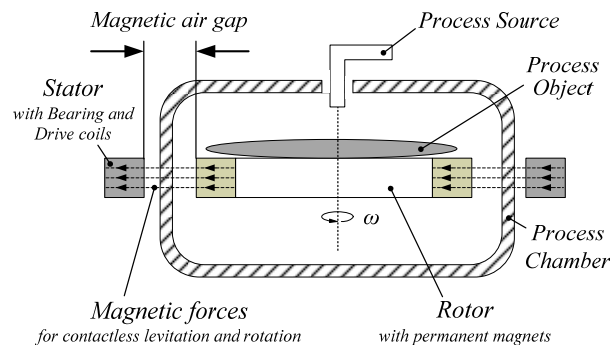


FIGURE 1: Schematic view of a typical industry spinning process that is hermetically sealed with a process chamber and a magnetically levitated rotor [1].

process chamber. This encapsulation ensures a particle-free and ultra-clean environment for the process.

While three degrees of freedom (radial displacements and rotation) are controlled actively, the remaining three degrees of freedom (axial displacement and tilting) are stabilized passively by reluctance forces [1] as shown in Figure 2. Besides the stable and vibration-free operation within the whole speed range the main challenge for these motors is to deliver a very high acceleration capability notwithstanding the large air gap in the range of several millimeters [4].

In the past, a lot of research has been done for these motors [4]-[7] in order to identify the most appropriate topology for accomplishing the required acceleration. However, little work has been done to evaluate the ideal number of motor phases, although of high importance for industrial praxis. Nowadays systems typically feature a two-phase bearing and a two-phase drive system powered by standard full bridges. The reason lies mainly in the fact that the two axes of the radial displacement are controlled with least effort regarding power electronics and sensors by a 2-phase bearing phase setup. In combination, typically also two drive phases (driven by full bridge topologies) are employed for generating the motor torque.

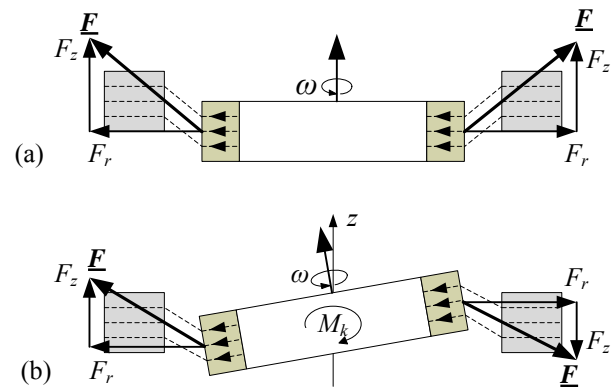


FIGURE 2: (a) Axial support and (b) stabilization against tilting of the rotor by passive magnetic forces in a bearingless slice motor [1].

However, 3-phase configurations seem to offer an interesting alternative, since intelligent power modules [8] with integrated features (such as short-circuit protection, temperature surveillance and integrated gate drivers) can be employed and a robust and compact power electronics setup is feasible. This three-phase concept can be applied for both the bearing and the drive system of the motor.

In this paper, a performance evaluation between the two-phase and the three-phase bearingless slice motor concept is undertaken, whereby the main emphasis will be put on the performance of the drive system. The comparison is based on general analytical calculations and 3D simulation data and is exemplified for typical specifications. The findings can be used for selecting the appropriate motor and power electronics topology for future systems.

MOTOR SETUP

In general, many different embodiments for the stator and rotor geometries are possible for the realization of a bearingless slice motor. The key parameters to describe a specific configuration are the number of stator claws k , the number of pole pairs of the rotor magnets p , and the number of phases for the drive windings m . Considering a certain minimum distance between the stator claws to insert the sensors and to avoid saturation effects [9], a certain maximum number of stator claws k can be placed. These k stator claws can be used for the drive windings as well as for the bearing windings, where the sequence can be chosen arbitrarily. One claw can even carry a combination of drive and bearing windings. For sake of simplicity and clarity this paper covers only configurations featuring only one coil per claw with an alternating bearing-drive sequence. This typically leads to a well distributed force and torque characteristic in all directions. With this, every second claw can be used for the drive windings, thus there are totally $k_D = k / 2$ claws available for the drive as shown in Figure 3.

For each application, the three parameters k , p and m have to be carefully chosen in order to fulfill given requirements. As will be shown, not every possible combination of k and p is suitable for both 2-phase and 3-phase systems.

Figure 4 shows an exemplary 2-phase configuration with $k = 8$ and $p = 11$. For illustration, current is only flowing in one drive phase D_1 and in one bearing phase B_1 in positive direction generating a magnetic flux as indicated, while the currents in the other drive and bearing phases are set to zero. For the specific angular rotor position this current generates a torque M_z in clockwise direction as well as a radial force F_x .

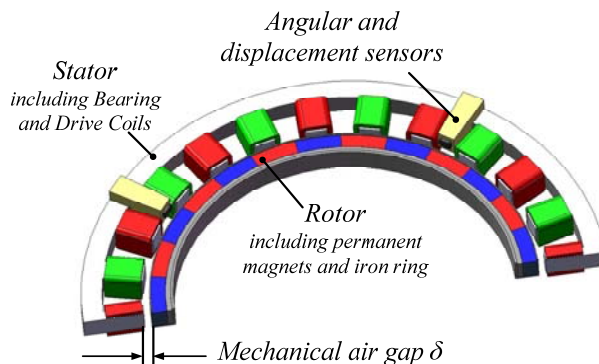


FIGURE 3: Schematic cut view of the stator with alternating coils for drive and bearing and rotor with alternately polarized permanent magnets.

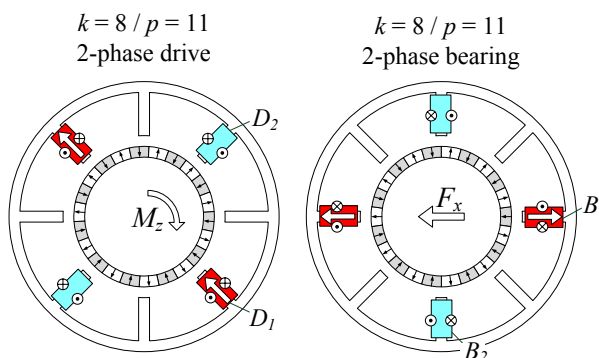


FIGURE 4: winding configuration and directions for a 2-phase system with $k = 8$ and $p = 11$. The directions of the magnetic field in case of a positive (in winding direction) current flowing in phase D_1 and B_1 , respectively, are shown.

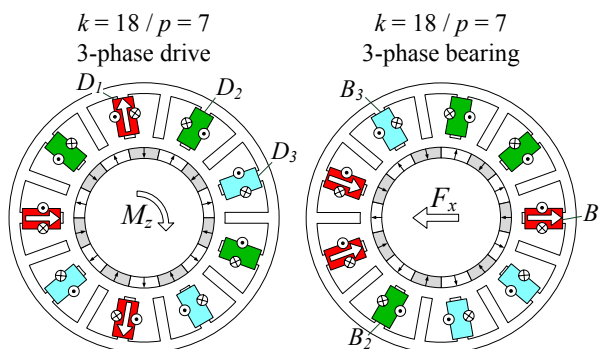


FIGURE 5: winding configuration and directions for a 3-phase system with $k = 18$ and $p = 7$. The directions of the magnetic field in case of a positive (in winding direction) current flowing in phase D_1 and B_1 , respectively, are shown.

For an angular rotation of 90° el. of the rotor an analog situation occurs for the second drive and bearing phase, generating again a torque M_Z as well as a radial force F_Y in positive y -direction.

This combination of k and p can only be used for 2-phase systems as there is no reasonable winding configuration with three phases possible. Another exemplary setup with $k = 18$ and $p = 7$ is shown in Figure 5, where a 3-phase drive and bearing winding can be realized, but no reasonable 2-phase configuration can be found. Again, it can be seen how a positive current in the drive phase D_1 and the bearing phase B_1 generates a torque M_Z and a radial force F_X , respectively.

As can be seen from these two exemplary cases, the number of pole pairs p can be higher (cf. Figure 4) or lower (cf. Figure 5) than the number of stator claws. Typically, good results in terms of maximum winding utilization and minimum cogging torque can be achieved, if there is neither a common divisor for k and p (for the drive system) nor for k and $(p+1)$ (for the bearing system [1]). Otherwise, the appearing cogging torque leads to a jerky rotation at low rotational speeds.

For a fair and meaningful performance comparison of 2-phase and 3-phase systems, a design with a claw number k and a number of pole pairs p has to be found, which is suitable for both 2-phase and 3-phase system. With this, the system driven by 2-phase drive windings can be compared directly to the same system driven by 3-phase drive windings.

A system fulfilling these requirements is with $k = 24$ stator claws and a rotor with $p = 13$ pole pairs. For this combination, winding configurations for the drive and bearing windings can be found both for the 2-phase (shown in Figure 6) and for the 3-phase system (shown in Figure 7). Both setups feature a very good winding utilization as well as a low cogging torque. Therefore, for the further calculations and experiments the two setups shown in Figure 6 and 7 are used to compare 2-phase and 3-phase winding concepts.

MODEL OF THE DRIVE SYSTEM

In order to compare the 2-phase and the 3-phase drive system, in the following, scaling laws of the drive system are derived from a simple model. With this, the acceleration capability can be compared for the two setups. For this model, it is assumed that for both the 2-phase as well as the 3-phase configuration semiconductors with the same ampacity $I_{PE,max}$ are utilized. Furthermore, sinusoidal drive currents and voltages are assumed and saturation effects are not considered for sake of simplicity.

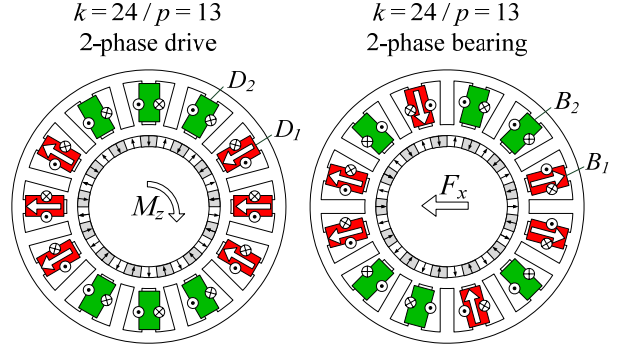


FIGURE 6: 2-phase winding configuration and directions for the prototype system with $k = 24$ and $p = 13$. The directions of the magnetic field in case of a positive (in winding direction) current flowing in phase D_1 and B_1 , respectively, are shown.

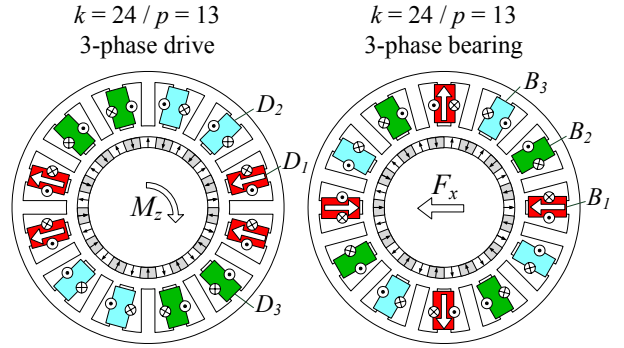


FIGURE 7: 3-phase winding configuration and directions for the prototype system. The directions of the magnetic field in case of a positive (in winding direction) current flowing in phase D_1 and B_1 , respectively, are shown.

For the calculation of the acceleration capability mainly two parameters are crucial:

1. The induced voltage $U_{ind,rms}$ (back EMF voltage) per phase, which is proportional to the induced voltage factor k_{Uind} according to

$$U_{ind,rms} = N_C \cdot n_R \cdot k_{Uind} \frac{k_D}{m} \quad (1)$$

with the number of turns N_C per claw, the rotational speed n_R in rpm, the number of drive claws k_D and the number of phases m (in our case 2 and 3, respectively). The factor k_{Uind} can be identified by 3D finite-element simulations of the setup and/or measured in an experimental setup.

2. The inductance per phase L is given by

$$L = \frac{k_D}{m} k_L \cdot N_C^2, \quad (2)$$

where $1/k_L$ is the reluctance of one coil placed at one of the k_D stator claws. Again, the parameter k_L can be identified by 3D electromagnetic simulations or measured on a practical setup.

In dependency of these two factors $k_{U_{ind}}$ and k_L the acceleration time to a desired rotation speed n_θ can be calculated (assuming field orientated control, i.e. induced voltage and impressed current being in phase) by

$$t_{acc} = \frac{J}{k_D \cdot k_{U_{ind}} \cdot N_C} \cdot \left(\frac{2\pi}{60}\right)^2 \cdot \int_0^{n_\theta} \frac{1}{I_{D,rms}(n_R)} dn_R, \quad (3)$$

whereby under the negligence of the coil resistance the drive current $I_{D,rms}$ is defined by

$$I_{D,rms}(n_R) = \frac{I_{PE,max}}{\sqrt{2}} \quad \text{for } \sqrt{2} \cdot I_{D,rms} > I_{PE,max}$$

and

$$I_{D,rms}(n_R) = \frac{60 \cdot \sqrt{U_{D,rms}^2 - U_{ind,rms}^2}}{2\pi \cdot n_R \cdot p \cdot L} \quad \text{for } \sqrt{2} \cdot I_{D,rms} < I_{PE,max}$$

with the maximum allowable power electronics current $I_{PE,max}$ and the specific applicable drive voltage $U_{D,rms}$. This correlation is shown in Figure 8. That means that above a certain rotational speed n_C the drive current (and thus the torque) is reduced due to the influence of the coil inductance L (cf. Figure 8) and the back EMF voltage.

If the number of coil windings is reduced in order to shift n_C up towards higher speeds (probably out of the

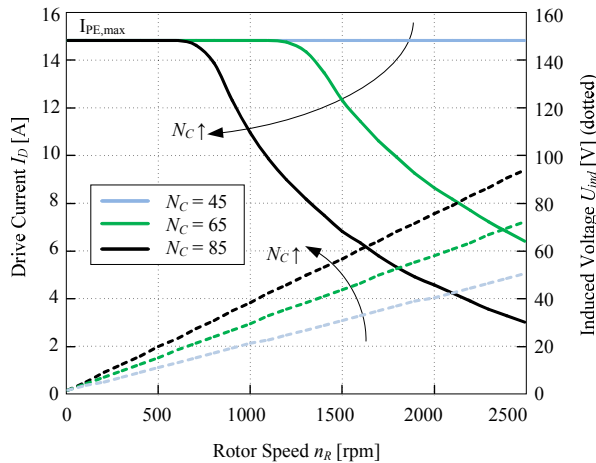


FIGURE 8: Calculated drive current I_D and induced voltage U_{ind} (dotted) in dependency of the rotor speed n_R for $U_{DC} = 300V$ and $I_{PE,max} = \sqrt{2} \cdot 15A$.

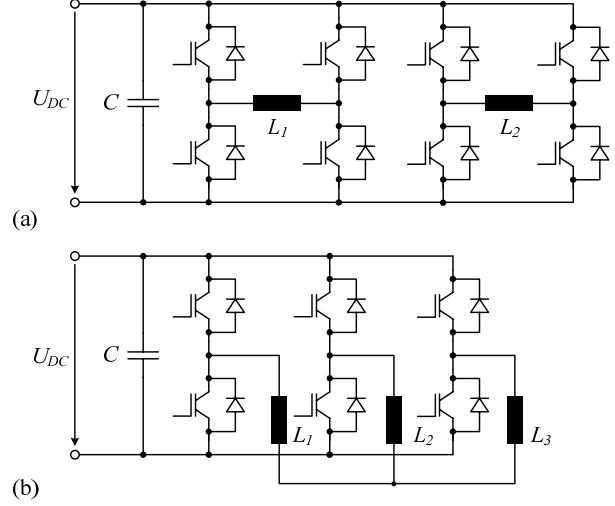


FIGURE 9: Power electronics inverter topology for the 2-phase (drive or bearing) system (a) with two full-bridges and for the 3-phase system (b) with three half-bridges in star connection.

operating speed range as it is the case for $N_C = 45$ in Figure 8) and to maximize the drive current $I_{D,rms}$, the induced voltage $U_{ind,rms}$ is reduced according to (1). Apparently, a minimum acceleration time is achieved by a compromise between high number of turns (high power at low speeds) and a low number of turns (high power at high speeds). Hence, the number of turns can be optimized for each configuration depending on the ratio between the factors $k_{U_{ind}}$ and k_L for a certain required rotation speed n_θ .

POWER ELECTRONICS SETUP

As mentioned in the introduction, bearingless motors typically use 2-phase winding setups for both the drive and the bearing system. Each phase is then driven by a full-bridge inverter circuit as shown in Figure 9(a). Alternatively, a 3-phase configuration is possible, with the three phases (both for the drive and for bearing system) being connected in star as shown in Figure 9(b).

Apparently, the power electronics for the 2-phase system is characterized by a higher number of required semiconductors than for the 3-phase system. In the latter case there are only three half-bridges needed due to the star-connection of the three phases, whereas two full-bridges are required for the 2-phase system, which correspond to four half-bridges. Hence, a factor ζ_E describing the power electronics effort can be defined by the ratio of the number n of half bridges:

$$\xi_E = \frac{n_{3ph}}{n_{2ph}} = 0.75. \quad (6)$$

However, the ratio of the power being delivered to the phases (assuming again the same ampacity of the power semiconductors) is different from this value. In the case of a full-bridge configuration as it is the case for the 2-phase system the available drive voltage $U_{D,rms}$ is given by

$$U_{D,rms} = \frac{U_{dc}}{\sqrt{2}} \quad (7)$$

and in the case of a three-phase star-connection

$$U_{D,rms} = \frac{U_{dc}}{\sqrt{6}}. \quad (8)$$

Thus, the voltage $U_{D,rms}$ over each of the drive coils is lower in the case of the 3-phase star-connection, as can be seen by comparing (7) and (8). In return, in case of the 3-phase concept one more phase contributes to the drive power. The total power of the 2-phase system is therefore given by

$$P_{2ph} = 2 \cdot U_{D,rms} \cdot I_{D,rms} = I_{D,rms} \frac{2}{\sqrt{2}} \cdot U_{dc} \quad (9)$$

and in the case of the 3-phase system by

$$P_{3ph} = 3 \cdot U_{D,rms} \cdot I_{D,rms} = I_{D,rms} \frac{3}{\sqrt{6}} \cdot U_{dc}. \quad (10)$$

With this, a power ratio ξ_P can be calculated as the ratio of the deliverable power value of the 3-phase to the 2-phase system:

$$\xi_P = \frac{P_{3ph}}{P_{2ph}} = \frac{\sqrt{3}}{2} = 0.87. \quad (11)$$

Thus, the 3-phase configuration delivers 13% less drive power to the system compared to the 2-phase full-bridge configuration (while having 25% less power electronics effort). However, for comparing the total drive performance of the two setups, the acceleration behavior over a certain specified rotational speed range has to be considered. This will be carried out in the subsequent section based on the model of the drive system that has been derived before.

PERFORMANCE COMPARISON

In order to compare the drive performance of the 3-phase and the 2-phase setup, an acceleration performance factor is introduced

$$\xi_A = \frac{1/t_{3ph}}{1/t_{2ph}} = \frac{t_{2ph}}{t_{3ph}}. \quad (12)$$

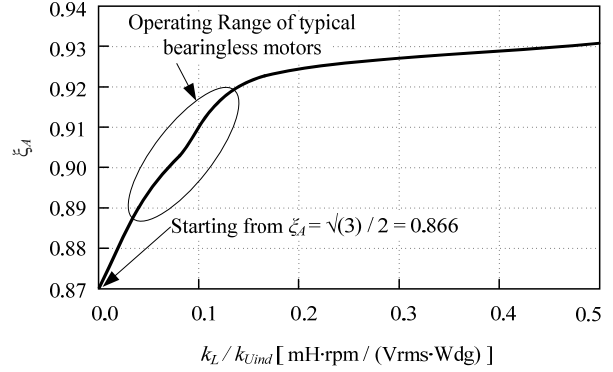


FIGURE 10: Acceleration performance factor in dependency factor ξ_A in dependency on the ratio of k_L / k_{Uind} .

As concluded before, the achievable acceleration time to a certain required rotational speed n_0 strongly depends on the selected number of drive turns N . Based on (1) to (5), for specific values of the induced voltage factor k_{Uind} , the coil inductance factor k_L , the number of phases m , the applicable drive voltage $U_{D,rms}$, the required rotation speed n_0 , the number of pole pairs p , and the maximum allowable current $I_{PE,max}$ always an optimum number of drive turns N_{opt} can be found. Now, the question arises, if this optimum number of turns automatically leads to an acceleration performance factor ξ_A being equal to the power ratio ξ_P .

As a detailed analysis shows, only the ratio k_L / k_{Uind} is of importance for the acceleration factor ξ_A . Figure 10 shows that for small values of the ratio the factor ξ_A is essentially identical with ξ_P . This is due to the fact that the inductance value is very small (resulting in a very steep decay of the drive current above n_c) so that the optimization of the number of turns leads to $n_0 = n_c$ and the maximum current can be driven over the whole speed range. For higher ratios of k_L / k_{Uind} the before-mentioned trade-off between high power at low speeds (high number of turns) and high power at high speeds (high number of turns) occurs. As can be seen in Figure 10, this effects a slight increase of the acceleration factor ξ_A , i.e. a relative improvement of the 3-phase setup compared with the 2-phase setup.

The typical ratio of k_L / k_{Uind} for bearingless motors lies in the range of 0.05 ... 0.15 [mH·rpm/(V_{rms}·Wdg)], resulting in $\xi_A = 0.89$... 0.92. With this, the star-connected 3-phase setup has about only 10% lower acceleration performance compared to the full-bridge 2-phase system, even though the power electronics effort is only 75%.

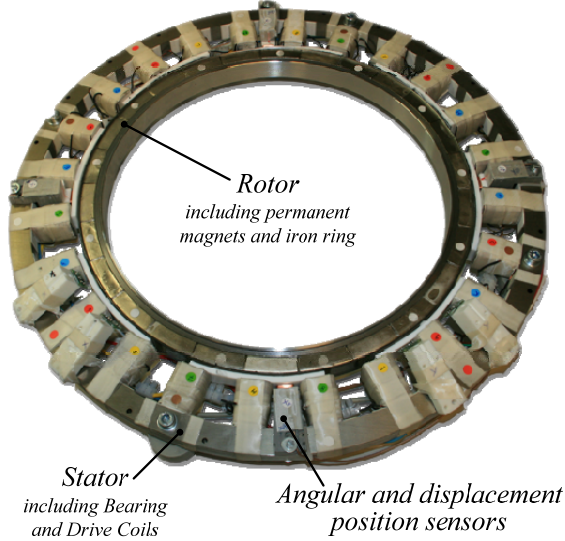


FIGURE 11: Prototype featuring $k = 24$ stator claws and a rotor with $p = 13$ pole pairs.

EXPERIMENTAL VERIFICATION

In order to verify the analytical considerations, a prototype has been designed and built, which allows to implement both 2-phase and 3-phase winding configurations. As previously mentioned, $k = 24$ stator claws and $p = 13$ pole pairs have been chosen for sake of a fair comparison. A photograph of the prototype system is shown in Figure 11 and characteristic key data is compiled in Table 1. Finally, the acceleration behavior of the 3-phase configuration is compared to the 2-phase setup for different run-ups up to specified maximum speed $n_0 = 2500$ rpm. It can be seen that they achieve very similar acceleration times. The acceleration performance factor according to (12) can be calculated for the maximum speed ($n_0 = 2500$ rpm) to $\zeta_A = 0.91$, which is in good accordance to the analytically calculated values in Figure 10 for the given value of $k_L / k_{Uind} = 0.065$ [mHrpm/(V_{rms}Wdg)].

CONCLUSION

This paper shows that 3-phase drive winding concepts may offer a good alternative to the conventionally used 2-phase concepts for bearingless motors. Although they have significantly less power electronics effort and offer the possibility to employ commercially available and highly compact intelligent power modules, they feature only a slightly lower acceleration performance than 2-phase setups. These findings can be used for further designs of bearingless slice motors.

TABLE 1: Design data of the experimental setup

Total Number of stator claws	k	24
Number of drive claws	k_D	12
Number of bearing claws	k_B	12
Number of pole pairs	p	13
Stator outer diameter	D	500 mm
Mechanical air gap	δ	7 mm
Rotor weight	m	3.1 kg
Radial stiffness	k_R	-95.3 N/mm
Axial stiffness	k_Z	20.0 N/mm
Force-current factor	k_I	18.5 mN/(AWdg)
Inductivity factor per coil	k_L	209.2 nH/Wdg ²
Voltage-speed factor	k_{Uind}	3.2 mVrms/(Wdg rpm)

2-phase system

Bearing phase winding number	N_B	12 x 65 turns
Drive phase winding numbers	N_D	12 x 55 turns

3-phase system

Bearing phase winding number	N_B	12 x 65 turns
Drive phase winding numbers	N_D	12 x 45 turns

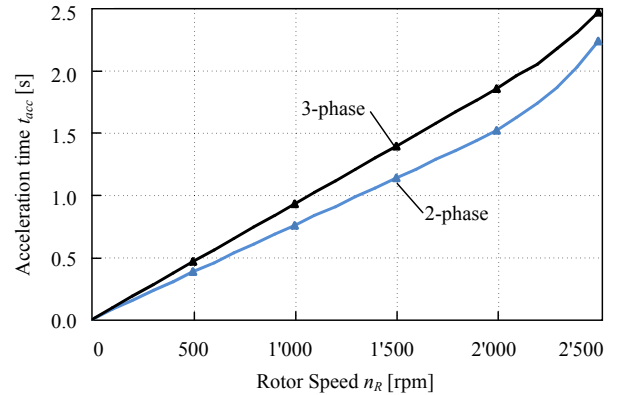


FIGURE 12: Acceleration performance results for the bearingless slice motor at hand with a 2-phase drive windings configuration compared to the same system with a 3-phase drive windings configuration. Each measurement point indicates the needed acceleration time from 0 rpm to the specified speed up to 2500 rpm.

REFERENCES

- [1] R. Schoeb, N. Barletta, "Principle and application of a bearingless slice motor", Proc. 5th Int. Symposium on Magnetic Bearings (ISMB5), Kanazawa (Japan), pp. 313-318, 1996.
- [2] Y. Chisti, M. Moo-Young, "Clean-in-place systems for industrial bioreactors: Design, validation and operation," *Journal of Industrial Microbiology and Biotechnology*, 1994.
- [3] J. Boehm, R. Gerber, J.R. Hartley, S. Whitley, "Development of active magnetic bearings for high speed rotors," *IEEE Trans. on Magnetics*, vol.26, no.5, pp.2544-2546, Sep. 1990.
- [4] P. Karutz, T. Nussbaumer, W. Gruber, J.W. Kolar, "The bearingless 2-level motor", Proc. 7th Int. Conf. Power Electron. and Drive Systems (PEDS'07), Bangkok, Thailand, Nov. 27-30, 2007.
- [5] S. Silber, W. Amrhein, P. Boesch, R. Schoeb, N. Barletta, "Design aspects of bearingless slice motors", *IEEE Trans. Mechatron.*, vol. 10, no. 6, pp. 611-617, Dec. 2005.
- [6] J. Amemiya, A. Chiba, D.G. Dorrell, T. Fukao, "Basic characteristics of a consequent-pole-type bearingless motor", *IEEE Trans. Magn.*, vol. 41, no. 1, pp. 82-89, Jan. 2005.
- [7] T. Schneeberger, J.W. Kolar, "Novel integrated bearingless hollow-shaft drive", Proc. 41st IEEE Ind. Appl. Conf. (IAS'06), Tampa, USA, Oct. 8-12, 2006.
- [8] International Rectifier: Integrated Hybrid IC IRA-MY30UP60B, Datasheet (2006).
- [9] P. Karutz, T. Nussbaumer, W. Gruber, J.W. Kolar, "Saturation effects in high acceleration bearingless slice motors", Proc. Int. Symp. Ind. Electron. (ISIE'08), Cambridge, UK, Jun. 30 – Jul. 2, 2008.